



HAL
open science

Field-Induced Dysprosium Single-Molecule Magnet Based on a Redox-Active Fused 1,10-Phenanthroline-Tetrathiafulvalene-1,10-Phenanthroline Bridging Triad

Bertrand Lefeuvre, Olivier Galangau, Jessica Flores Gonzalez, Vincent Montigaud, Vincent Dorcet, Lahcone Ouahab, Boris Le Guennic, Olivier Cador, Fabrice Pointillart

► To cite this version:

Bertrand Lefeuvre, Olivier Galangau, Jessica Flores Gonzalez, Vincent Montigaud, Vincent Dorcet, et al.. Field-Induced Dysprosium Single-Molecule Magnet Based on a Redox-Active Fused 1,10-Phenanthroline-Tetrathiafulvalene-1,10-Phenanthroline Bridging Triad. *Frontiers in Chemistry*, 2018, 6, pp.552. 10.3389/fchem.2018.00552. hal-01973910

HAL Id: hal-01973910

<https://univ-rennes.hal.science/hal-01973910>

Submitted on 16 Jul 2019

HAL is a multi-disciplinary open access archive for the deposit and dissemination of scientific research documents, whether they are published or not. The documents may come from teaching and research institutions in France or abroad, or from public or private research centers.

L'archive ouverte pluridisciplinaire **HAL**, est destinée au dépôt et à la diffusion de documents scientifiques de niveau recherche, publiés ou non, émanant des établissements d'enseignement et de recherche français ou étrangers, des laboratoires publics ou privés.



Field-Induced Dysprosium Single-Molecule Magnet Based on a Redox-Active Fused 1,10-Phenanthroline-Tetrathiafulvalene-1,10-Phenanthroline Bridging Triad

Bertrand Lefeuvre, Olivier Galangau, Jessica Flores Gonzalez, Vincent Montigaud, Vincent Dorcet, Lahcène Ouahab, Boris Le Guennic, Olivier Cador* and Fabrice Pointillart*

Univ Rennes, CNRS, ISCR (Institut des Sciences Chimiques de Rennes)-UMR 6226, Rennes, France

OPEN ACCESS

Edited by:

Hitoshi Ishida,
Kitasato University, Japan

Reviewed by:

Sukhendu Mandal,
Indian Institute of Science Education
and Research, Thiruvananthapuram,
India

Juan Manuel Herrera,
Universidad de Granada, Spain

*Correspondence:

Olivier Cador
olivier.cador@univ-rennes1.fr
Fabrice Pointillart
fabrice.pointillart@univ-rennes1.fr

Specialty section:

This article was submitted to
Inorganic Chemistry,
a section of the journal
Frontiers in Chemistry

Received: 25 May 2018

Accepted: 25 October 2018

Published: 13 November 2018

Citation:

Lefeuvre B, Galangau O, Gonzalez JF,
Montigaud V, Dorcet V, Ouahab L,
Le Guennic B, Cador O and
Pointillart F (2018) Field-Induced
Dysprosium Single-Molecule Magnet
Based on a Redox-Active Fused
1,10-Phenanthroline-
Tetrathiafulvalene-1,10-Phenanthroline
Bridging Triad. *Front. Chem.* 6:552.
doi: 10.3389/fchem.2018.00552

Tetrathiafulvalene and 1,10-phenanthroline moieties present, respectively remarkable redox-active and complexation activities. In this work, we investigated the coordination reaction between the bis(1,10-phenanthro[5,6-b])tetrathiafulvalene triad (**L**) and the Dy(hfac)₃·2H₂O metallo precursor. The resulting {[Dy₂(hfac)₆(**L**)]·CH₂Cl₂·C₆H₁₄]₃ (**1**) dinuclear complex showed a crystal structure in which the triad **L** bridged two terminal Dy(hfac)₃ units and the supramolecular co-planar arrangement of the triads is driven by donor-acceptor interactions. The frequency dependence of the out-of-phase component of the magnetic susceptibility highlights three distinct maxima under a 2000 Oe static applied magnetic field, a sign that **1** displays a Single-Molecule Magnet (SMM) behavior with multiple magnetic relaxations. *Ab initio* calculations rationalized the Ising character of the magnetic anisotropy of the Dy^{III} ions and showed that the main anisotropy axes are perpendicular to the co-planar arrangement of the triads. Single-crystal rotating magnetometry confirms the orientation of the main magnetic axis. Finally combining structural analysis and probability of magnetic relaxation pathways through Quantum Tunneling of the Magnetization (QTM) vs. excited states (Orbach), each Dy^{III} center has been attributed to one of the three observed magnetic relaxation times. Such coordination compound can be considered as an ideal candidate to perform redox-magnetic switching.

Keywords: tetrathiafulvalene, triads, dysprosium, single-molecule magnet, ab initio calculations

INTRODUCTION

Single-Molecule Magnets (SMMs) are intensively studied for more than 25 years due to their potential applications in high density data storage, quantum computing, and spintronics (Leuenberger and Loss, 2001; Gatteschi et al., 2006; Lehmann et al., 2007; Bogani and Wernsdorfer, 2008; Mannini et al., 2009; Ganzhorn et al., 2013). Especially the interest for lanthanide ions has

quickly grown during the last decade due to their high magnetic moment and strong magnetic anisotropy making them potential candidates for the elaboration of SMMs (Benelli and Gatteschi, 2002; Sessoli and Powell, 2009; Rinehart and Long, 2011; Woodruff et al., 2013; Liddle and van Slageren, 2015; Goodwin et al., 2017; Guo et al., 2017; Pointillart et al., 2017; Gupta and Murugavel, 2018). Since most lanthanide centers are luminescent (Piguet and Bünzli, 1999; Comby and Bünzli, 2007), the use of such element pushes up the interest of both chemist and physicist communities for luminescent SMMs with proper correlation between optical and magnetic properties (Cucinotta et al., 2012; Long et al., 2012; Ehama et al., 2013; Yamashita et al., 2013; Ren et al., 2014; Yi et al., 2014; Pointillart et al., 2015c). In a general manner, the interest is focused on multi-properties SMM (Long et al., 2015; Ou-Yang et al., 2016), and thus redox active SMMs could be designed using tetrathiafulvalene(TTF)-based ligands (da Cunha et al., 2013; Gao et al., 2013, 2014; Pointillart et al., 2013b; Soussi et al., 2015). Obviously the design of such molecular objects implies modifications of the TTF core with various acceptor groups (Sessoli and Powell, 2009; Pointillart et al., 2013a) in order to guaranty the coordination reaction with the lanthanide ions. Among the plethora of possible decorations of the TTF fragment, the 1,10-phenanthroline (phen) is an excellent choice to construct donor-acceptor (D-A) systems (Jia et al., 2007; Keniley et al., 2010, 2013; Qin et al., 2011). Their association with metallic precursors as led already to the observation of auspicious optical (Dupont et al., 2013; Lapadula et al., 2015) and magnetic (Pointillart et al., 2015b, 2016) properties. Even more promising are the acceptor-donor-acceptor (A-D-A) triads, such as bis-(quinoxaline)-TTF (Nishida et al., 2006), bis(tetracyanoquinodimethane)-TTF (Otón et al., 2011a), bis(naphthoquinone)-TTF (Otón et al., 2011b), bis(pyrazine)-TTF (Schuler et al., 2014), bis-(dipyrido[3,2-a:2',3'-c]phenazine)-TTF (Jia et al., 2014), and bis(bistert-butyl-o-quinone)-TTF (Kuropatov et al., 2010) because the majority of them offers the possibility to bridge two metallic units which could be optically and magnetically active. In other words, A-D-A triads where A is a phen fragment and D a TTF moiety could play the role of a bridging unique redox-switch between two multi-properties units. Few triads involving the phen moiety are already available in the literature such as the bis-(dipyrido[3,2-a:2',3'-c]phenazine)-TTF (Jia et al., 2014) and Bis(1,10-phenanthro[5,6-b])tetrathiafulvalene (Chen et al., 2016).

In these lines, the latter triad was selected to bridge two SMM units as it could be readily obtained in a few synthetic steps. Thus the coordination reaction between the $\text{Dy}(\text{hfac})_3 \cdot 2\text{H}_2\text{O}$ units and the bis(1,10-phenanthro[5,6-b])tetrathiafulvalene triad (**L**) leads to the formation of a dinuclear complex of formula $\{[\text{Dy}_2(\text{hfac})_6(\text{L})] \cdot \text{CH}_2\text{Cl}_2 \cdot \text{C}_6\text{H}_{14}\}_3$ (**1**). The crystallographic structure highlights the role of bridge of the triad between the two $\text{Dy}(\text{hfac})_3$ units while the dynamic magnetic measurements show a field-induced multi-SMM behavior due to the six crystallographically independent Dy^{III} centers. The magnetic properties are fully rationalized using SA-CASSCF/SI-SO calculations.

MATERIALS AND METHODS

General

The precursor $\text{Dy}(\text{hfac})_3 \cdot 2\text{H}_2\text{O}$ ($\text{hfac}^- = 1,1,1,5,5,5$ -hexafluoroacetylacetonate anion) (Richardson et al., 1968) and the 1,3-dithiole-2-thione[4,5-f][1,10-phenanthroline] (Qin et al., 2011) compound were synthesized following previously reported methods. All other reagents were purchased from Aldrich Co., Ltd. and used without further purification.

Single crystal of **1** was mounted on a APEXIII D8 VENTURE Bruker-AXS diffractometer for data collection (Mo K_α radiation source, $\lambda = 0.71073 \text{ \AA}$), from the Centre de Diffractométrie (CDIFX), Université de Rennes 1, France (**Table 1**). Structure was solved with a direct method using the SHELXT program (Sheldrick, 2015a) and refined with a full matrix least-squares method on F using the SHELXL-14/7 program (Sheldrick, 2015b). Complete crystal structure results as a CIF file including bond lengths, angles, and atomic coordinates are deposited as Supporting Information.

The elemental analyses of the compounds were performed at the Centre Régional de Mesures Physiques de l'Ouest, Rennes. Cyclic voltammetry was carried out in dried and degassed CH_2Cl_2 solution, containing 0.1 M $\text{N}(\text{C}_4\text{H}_9)_4\text{PF}_6$ as supporting electrolyte. Voltammograms were recorded at 100 mVs^{-1} at a platinum disk electrode. The potentials were measured vs. a saturated calomel electrode (SCE). The dc magnetic susceptibility measurements were performed on solid polycrystalline samples with a Quantum Design MPMS-XL SQUID magnetometer between 2 and 300 K under an applied magnetic field of 0.2 kOe for temperatures of 2–20 K, 2 kOe between 20 and 80 K and 10 kOe above. These measurements were all corrected for the diamagnetic contribution as calculated with Pascal's constants.

TABLE 1 | X-ray crystallographic data for **1** (CCDC 1826960).

Compounds	$\{[\text{Dy}_2(\text{hfac})_6(\text{L})] \cdot \text{CH}_2\text{Cl}_2 \cdot \text{C}_6\text{H}_{14}\}_3$ (1)
Formula	$\text{C}_{189}\text{H}_{102}\text{Cl}_6\text{Dy}_6\text{F}_{108}\text{N}_{12}\text{O}_{36}\text{S}_{12}$
$F_w/\text{g}\cdot\text{mol}^{-1}$	6741.24
Crystal system	triclinic
Space group	P-1 ($\text{N}^{\circ}2$)
Cell parameters	$a = 20.507(8) \text{ \AA}$ $b = 20.492(7) \text{ \AA}$ $c = 33.957(13) \text{ \AA}$ $\alpha = 93.123(12)^\circ$ $\beta = 96.248(13)^\circ$ $\gamma = 119.224(10)^\circ$
Volume/ \AA^3	12284.0(80)
Z	2
T/K	150 (2)
radiation	Mo K_α
2θ range/ $^\circ$	$4.10 \leq 2\theta \leq 56.37$
$\rho_{\text{calc}}/\text{g}\cdot\text{cm}^{-3}$	1.823
μ/mm^{-1}	2.117
Number of reflections	375,353
Independent reflections	53,657
R_{int}	0.1276
$F_o^2 > 2\sigma(F_o)^2$	39,102
Number of variables	2,896
GOOF	1.129
$R_1, \omega R_2$	0.1396, 0.3716

The ac magnetic susceptibility measurements were performed on both Quantum Design MPMS-XL SQUID and Quantum Design PPMS magnetometers.

Wavefunction-based calculations were carried out on the partially-optimized structure of a mononuclear model complex (*vide infra*) by using the SA-CASSCF/RASSI-SO approach, as implemented in the MOLCAS quantum chemistry package (versions 8.0; Aquilante et al., 2016). In this approach, the relativistic effects are treated in two steps on the basis of the Douglas–Kroll Hamiltonian. First, the scalar terms were included in the basis-set generation and were used to determine the spin-free wave functions and energies in the complete active space self-consistent field (CASSCF) method (Roos et al., 1980). Next, spin-orbit coupling was added within the restricted-active-space state-interaction (RASSI-SO) method, which uses the spin-free wave functions as basis states (Malmqvist and Roos, 1989; Malmqvist et al., 2002). The resulting wave functions and energies are used to compute the magnetic properties and g-tensors of the lowest states from the energy spectrum by using the pseudospin $S = 1/2$ formalism implemented in the SINGLE-ANISO routine (Chibotaru et al., 2008; Chibotaru and Ungur, 2012). Cholesky decomposition of the bielectronic integrals was employed to save disk space and speed-up the calculations (Aquilante et al., 2008). The active space in the CASSCF calculation consisted of the nine 4f electrons of the Dy^{III} ion spanning the seven 4f orbitals, i.e., CAS(9,7)SCF. State-averaged CASSCF calculations were performed for all of the sextets (21 roots), all of the quadruplets (224 roots), and 300 out of the 490 doublets (due to software limitations) of the Dy(III) ion. Twenty one sextets, 128 quadruplets, and 107 doublets were mixed through spin-orbit coupling in RASSI-SO. All atoms were described by ANO-RCC basis sets (Roos et al., 2004, 2005, 2008). The following contractions were used: [8s7p4d3f2g1h] for Dy, [4s3p2d1f] for the O and N atoms [3s2p1d] for the C and F atoms, [4s3p1d] for the S atoms and [2s] for the H atoms. DFT geometry optimization has been performed on model complexes for the 6 asymmetric Dy centers. The atomic positions of the molecule were extracted from the X-ray crystal structure. For each Dy center, the corresponding dimer unit has been cut in half at

the bridging C-C double bond, the corresponding truncated C atom being replaced by a H atom (see **Figure S10**). In the optimization, the Dy(III) center was replaced by Y(III). Only the H and F positions were optimized while all the other positions were kept frozen. The calculations were carried using the PBE0 (Perdew et al., 1996; Adamo and Barone, 1999) hybrid functional implemented in the Gaussian 09 (revision D.01) package (Frisch et al., 2013). The “Stuttgart/Dresden” basis sets and effective core potentials were used to describe the yttrium atom (Dolg et al., 1993) while the other atoms were described with SVP basis sets (Weigend and Ahlrichs, 2005).

Synthesis

Bis(1,10-phenanthro[5,6-b])tetrathiafulvalene triad (**L**)

L was synthesized by modifying the published method (Chen et al., 2016). The 1,3-dithiole-2-thione[4,5-f][1,10-phenanthroline] was used instead of the 1,3-dithiole-2-one[4,5-f][1,10-phenanthroline] compound in order to cancel the oxidation step of the thione in one derivative. Yield: 45%.

{[Dy₂(hfac)₆(L)]·CH₂Cl₂·C₆H₁₄}₃ (**1**)

Eleven milligram of **L** (0.022 mmol) were added to 20 ml of 1,2-dichloroethane. The suspension was heated to reflux and then a solution of 10 mL of 1,2-dichloroethane containing 35 mg of Dy(hfac)₃·2H₂O (0.043 mmol) was added. After 6 h of reflux, the 1,2-dichloroethane was eliminated under vacuum and the residue was dissolved in CH₂Cl₂. *n*-hexane was layered on the CH₂Cl₂ solution of **1** in the dark to give red single crystals suitable for X-ray diffraction study. I.R. bands (KBr): 2965, 1651, 1564, 1538, 1499, 1465, 1260, 1216, 1147, 1100, 806, 662, and 588 cm⁻¹. Anal. Calcd (%) for C₁₈₉H₁₀₂Cl₆Dy₆F₁₀₈N₁₂O₃₆S₁₂ (**1**): C 33.64, H 1.51, N 2.49; found: C 33.71, H 1.66 N, 2.37.

RESULTS AND DISCUSSION

Structural Analysis

The X-ray crystallographic data for compound **1** are given in **Table 1**. It crystallizes in the P-1 (*N*²) triclinic space group.

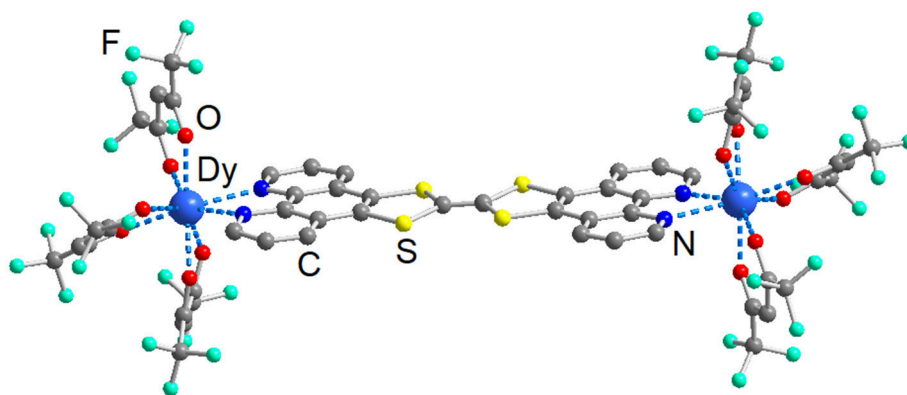
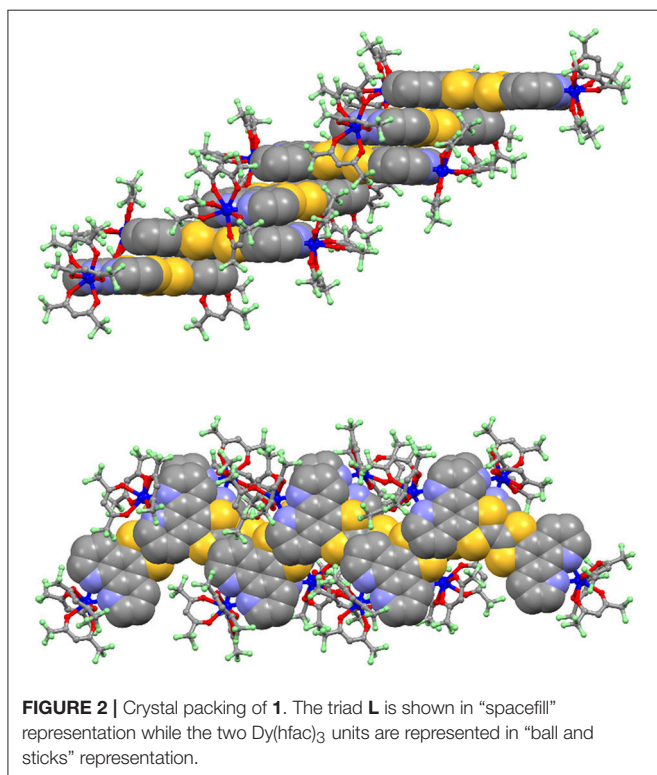


FIGURE 1 | Molecular structure of a dinuclear complex which composed **1**. Carbon (C, gray); fluorine (F, green); oxygen (O, red); nitrogen (N, blue); sulfur (S, yellow), and dysprosium (Dy, dark blue).

The asymmetric unit is composed by two dinuclear complexes of formula $[\text{Dy}_2(\text{hfac})_6(\text{L})]$, two half dinuclear complexes, three dichloromethane and three *n*-hexane molecules of crystallization. In other words, six crystallographically independent Dy^{III} centers are present in the molecular structure (Figure S1). All the Dy^{III} centers are linked to three hfac^- anions and one **L** ligand giving an N_2O_6 surrounding with a D_{4d} symmetry (square antiprism) for Dy1, D_{2d} symmetry for Dy2-Dy5 and an intermediate symmetry between D_{2d} and C_{2v} for Dy6. The distortion is visualized by continuous shape measures performed with SHAPE 2.1 (Table S1; Llunell et al., 2013). The two 1,10-phenanthroline coordination sites are occupied by $\text{Dy}(\text{hfac})_3$ units and **L** plays the role of bridge between two $\text{Dy}(\text{hfac})_3$ units (Figure 1).

As we expect for such large and extended aromatic ligands, **L** is planar offering optimal stacks in the crystals along the *c* unit cell direction. The molecular planes in the stack are coplanar (top part of Figure 2) but they are slightly shifted (or/and rotated of an angle ranging from 83 to 102°) relative to each other to guaranty efficient π - π interactions despite of the steric hindrance of the $\text{Dy}(\text{hfac})_3$ units (bottom part of Figure 2). No bent structures are obtained and the charge sensitive central C=C bond is found to be in average 1.335 Å, corresponding to neutral form of the TTF ligand part. Complementary interactions such as $\text{S} \cdots \text{N}$ or $\text{S} \cdots \text{S}$ might also play a role in the crystal packing. The dithiol sulfur atoms from the upper molecule are localized above the nitrogen atoms of the phenanthroline moiety of the lower one. The $\text{S} \cdots \text{N}$ distances range from 3.681 to 3.812 Å which is close to the



sum of the van der Waals radii (3.550 Å). Few $\text{S} \cdots \text{S}$ contacts are also identified with distances ranging from 3.871 to 4.141 Å. The minimal interplanar distance in the stack is 3.301 Å, suggesting the driving forces for the formation of stacks could be these acceptor-donor intermolecular interactions (bottom part of Figure 2).

To investigate sample homogeneity, PXRD was performed on crystalline powder of **1** (see Figure S2 for comparison between simulated and experimental PXRD pattern). Unfortunately, the powder showed a drastic loss of crystallinity character, probably due to solvents evaporation during the measurement (*vide infra*).

Electrochemical Properties

In contrast with the poor solubility of **L** in most common organic solvents, complex **1** is well soluble in CH_2Cl_2 and its redox properties could be investigated by cyclic voltammetry (Figure S3). The cyclic voltammogram shows two mono-electronic oxidations at 0.87 V and 1.22 V for the first and second oxidations, corresponding to the formation of a radical cation and a dication TTF fragment, respectively (Table 2).

These values are found very close to those reported by Zuo et al (Chen et al., 2016). The reversibility of the electrochemical properties is a clear evidence of the complex stability, meaning that almost no de-coordination seems to occur once **L** is converted to its radical cationic form, under these conditions. In addition, such results attest the reversibility of the oxidation potentials and the redox-activity of ligand (**L**) after complexation.

Magnetic Properties

The static magnetic properties were determined by measuring the thermal dependence of the magnetic susceptibility (χ_M) between 2 and 300 K (Figure 3A). The room temperature of the $\chi_M T$ product is equal to 27.86 $\text{cm}^3 \text{K mol}^{-1}$ i.e., an average value of 13.93 $\text{cm}^3 \text{K mol}^{-1}$ per $\text{Dy}(\text{III})$ center. Such value is in agreement with the expected value 14.17 $\text{cm}^3 \text{K mol}^{-1}$ for a $\text{Dy}(\text{III})$ free ion (${}^6\text{H}_{15/2}$, $g = 4/3$; Kahn, 1993). The $\chi_M T(T)$ curve monotonically decreases due to the depopulation of the M_J states until 2 K where the $\chi_M T$ product reaches the value of 22.50 $\text{cm}^3 \text{K mol}^{-1}$. At 2 K, the field dependence of the magnetization shows a classic behavior with a value of 10.54 $\text{N}\beta$ (31.61 $\text{N}\beta$ for the six Dy^{III} , Figure S3) at 50 kOe which is close to the expected value of 10 $\text{N}\beta$ for an Ising ground state of the dinuclear complex.

The dynamic magnetic properties were probed by measuring the frequency dependence of the magnetic susceptibility. Such

TABLE 2 | Oxidation potentials (V vs SCE, $n\text{Bu}_4\text{NPF}_6$, 0.1 M in CH_2Cl_2 at 100 $\text{mV}\cdot\text{s}^{-1}$) of the ligand **L** and complex $[\text{Dy}(\text{hfac})_3(\text{L})]\cdot\text{CH}_2\text{Cl}_2$.

	$E_{1/2}^1/\text{V}$		$E_{1/2}^2/\text{V}$	
	$\text{Ox}E_{1/2}^1$	$\text{Red}E_{1/2}^1$	$\text{Ox}E_{1/2}^2$	$\text{Red}E_{1/2}^2$
1	0.944	0.790	1.310	1.120

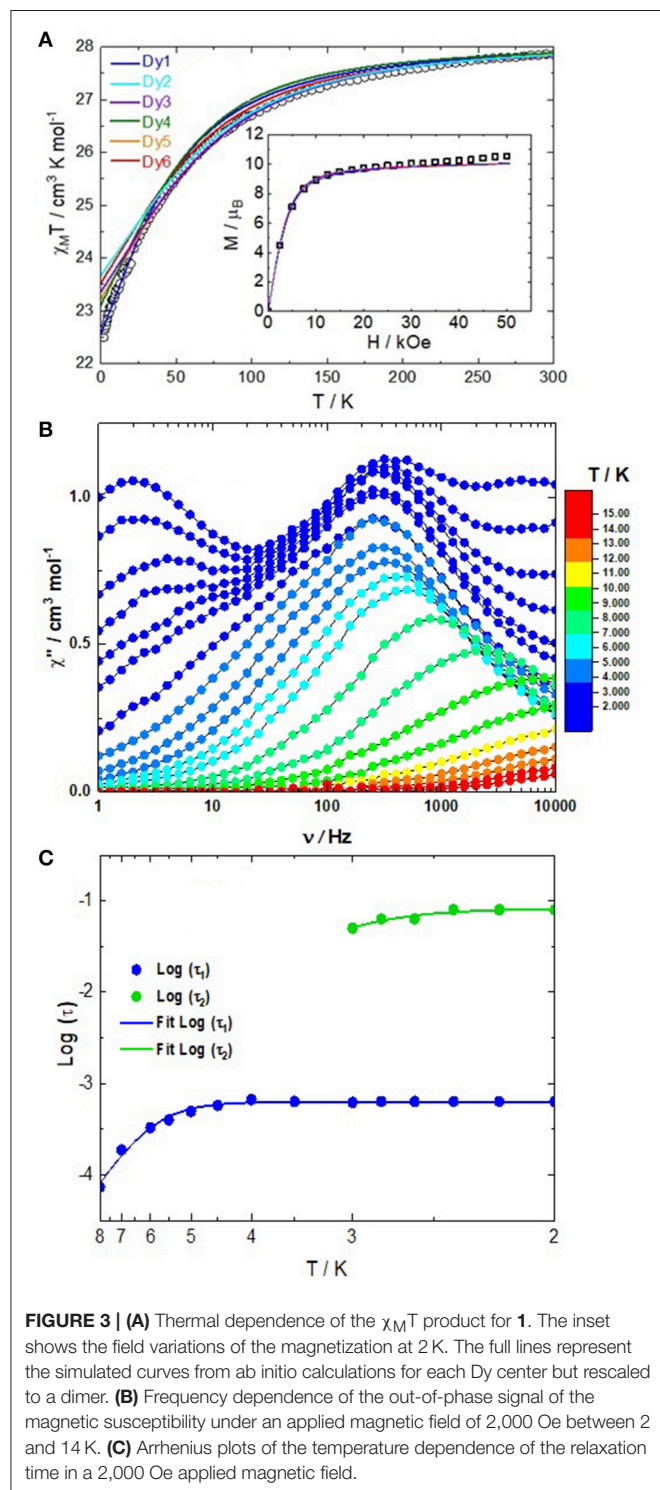
measurements only show an out-of-phase component of the magnetic susceptibility at high frequency and thus no maxima were observed in the experimental window at zero applied field. Consequently a scan field of the magnetic susceptibility at 2 K between 0 and 2,000 Oe was performed (Figure S4) in order to determine the optimal field to cancel the zero-field Quantum

Tunneling of the Magnetization (QTM; Gatteschi and Sessoli, 2003; Ishikawa et al., 2005a) and both dipolar and hyperfine interactions (Ishikawa et al., 2005b; Guo et al., 2011; Pointillart et al., 2015a). Under an applied magnetic field, few out-of-phase magnetic susceptibility maxima shift in the experimental window and could be attributed to the crystallographically different Dy(III) centers. At the optimal DC field of 2,000 Oe, three maxima were observed at 2 K (3 Hz, 315 Hz and 5,000 Hz, Figure 3B) whereas six different Dy^{III} ions have been identified in the crystal structure. It is worth noticing that the three sets of data have almost the same intensity meaning that the same number of Dy(III) are involved in each of them. The frequency dependence of the magnetic susceptibility under 2,000 Oe field and at various temperatures (Figure 3B and Figures S5–S7) confirmed the multiple relaxation behavior of **1**. Such a multi-peak magnetic response renders the fitting of the Arrhenius plots with an extended Debye model quite problematic (Figure S8). The dependence of the relaxation time (τ) with the temperature was represented considering the maxima of the out-of-phase susceptibility curves at each temperature. We manually selected the frequencies maxima to plot $\log(\tau)$ vs. T (Figure 3C). The Arrhenius data was fully extracted for the intermediate relaxation time (blue plots, called τ_1) while the Arrhenius plot was extracted at low temperature for the metal center(s) which display(s) the slowest magnetic relaxation time (green plots, called τ_2) and finally no Arrhenius was extracted for the metal center(s) which display(s) the fastest magnetic relaxation time because the maxima shift at too high frequency for $T > 2$ K. The Arrhenius plot deviates from the linearity at low temperature suggesting the coexistence of more than one relaxation process (Guo et al., 2010; Zhang et al., 2015, 2016; Lu et al., 2017; Zhu et al., 2019). The Arrhenius plot was fitted using a combination of Orbach relaxation ($\tau^{-1} = \tau_0^{-1} \exp(-\Delta/T) + \tau_{\text{IT}}^{-1}$) (Cole and Cole, 1941), which provided an energy barrier of $\Delta = 48(2)$ cm^{-1} and $\tau(1)_0 = 2.37(10) \times 10^{-7}$ s and remaining QTM. A tentative fit of the Arrhenius plot for τ_2 gave $\Delta = 32(3)$ cm^{-1} and $\tau(2)_0 = 3.12(46) \times 10^{-7}$ s and remaining QTM. Nevertheless, the existence of Raman (Orbach, 1961a,b; Scott and Jeffries, 1962; Abragam and Bleaney, 1970; Shrivastava, 1983), and/or Direct (Orbach, 1961a,b; Scott and Jeffries, 1962; Abragam and Bleaney, 1970; Shrivastava, 1983) processes cannot be excluded.

Rotating single-crystal magnetometry allows to determine experimentally the average susceptibility tensor. The angular dependence of the magnetization was measured at 2 K in three orthogonal planes of an oriented single crystal. The molar magnetic susceptibility was then fitted with

$$\chi_M = \frac{M}{H} = \chi_{\alpha\alpha} \cos^2\theta + \chi_{\beta\beta} \sin^2\theta + 2\chi_{\alpha\beta} \sin\theta \cos\theta$$

where α and β are the directions X, Y, and Z (Figure S9) in a cyclic permutation and θ is the angle between H and α . In the effective spin 1/2 formalism, the largest principal value of the g- tensor is equal to 16.53, close to the tabulated value (20.00) for a purely axial magnetic moment. In order to rationalize the experimental observations, ab-initio calculations (SA-CASSCF/SI-SO) were performed (see



Computational details, **Figure S11**). The crystal field splitting, g-tensor components and wavefunction composition for each Kramers's Doublet of the ground-state multiplet (${}^6H_{15/2}$) for the six Dy(III) ions were determined (**Table 3** and **Tables S2–S7**).

The calculated crystal field splittings of the ground multiplet state lead to a calculated χ_{MT} product, averaged over the six positions, which is perfectly in agreement with the experimental data (**Figure S10**). The composition of the ground doublet reproduces finely the experimental magnetization at 2 K. As expected, an Ising type anisotropy with the largest g value ranging from 18.99 to 19.46 (**Table 3**) was found with the orientation of the main magnetic axis perpendicular to the plane formed by the nitrogen atoms (**Figure 4**) and the metallic center. In other words, the anisotropy axis direction is positioned along

the most charged direction of the coordination polyhedral as already observed in several N_2O_6 environments (da Cunha et al., 2013; Pointillart et al., 2015b; Ou-Yang et al., 2016; Speed et al., 2017). These are in agreement with the experimental data for the orientation of the anisotropy axes, in which the g-value is slightly smaller due to the contribution of all the Dy atoms forming the unit cell. The ground doublet state is mainly composed of the $M_J = \pm 15/2$ doublet with small $M_J = \pm 11/2$ contributions suggesting the possibility to have magnetic relaxation through QTM. The calculated energy gaps between the ground doublet state and the first excited doublet state range from 96.4 to 146 cm^{-1} . Thus the calculations allow to rationalize the SMM behavior (at least under an applied magnetic field) but the activated energy barrier is overestimated probably because the intermolecular and hyperfine interactions

TABLE 3 | Computed energies, g-tensor components and wavefunction composition for the ground doublet state (GD) and 1st Excited State (ES) of the ground-state multiplet for the six Dy(III) centers in **1**.

		Energy (cm^{-1})	g_x	g_y	g_z	Wavefunction composition*
Dy1	GD	0	0.08	0.15	18.99	$0.86 \pm 15/2\rangle + 0.11 \pm 11/2\rangle$
	1st ES	96.4	1.19	2.52	13.82	$0.56 \pm 13/2\rangle + 0.24 \pm 9/2\rangle + 0.09 \pm 5/2\rangle$
Dy2	GD	0	0.01	0.01	19.46	$0.93 \pm 15/2\rangle + 0.07 \pm 11/2\rangle$
	1st ES	146.0	0.17	0.25	15.64	$0.75 \pm 13/2\rangle + 0.19 \pm 9/2\rangle$
Dy3	GD	0	0.01	0.02	19.33	$0.91 \pm 15/2\rangle + 0.08 \pm 11/2\rangle$
	1st ES	139.0	0.16	0.26	14.92	$0.60 \pm 13/2\rangle + 0.27 \pm 9/2\rangle + 0.08 \pm 5/2\rangle$
Dy4	GD	0	0.02	0.05	19.23	$0.89 \pm 15/2\rangle + 0.10 \pm 11/2\rangle$
	1st ES	111.1	0.28	0.54	14.60	$0.60 \pm 13/2\rangle + 0.26 \pm 9/2\rangle + 0.07 \pm 5/2\rangle$
Dy5	GD	0	0.01	0.02	19.27	$0.90 \pm 15/2\rangle + 0.09 \pm 11/2\rangle$
	1st ES	133.4	0.41	0.83	14.16	$0.58 \pm 13/2\rangle + 0.27 \pm 9/2\rangle + 0.13 \pm 5/2\rangle$
Dy6	GD	0	0.01	0.01	19.40	$0.92 \pm 15/2\rangle + 0.07 \pm 11/2\rangle$
	1st ES	128.4	0.19	0.38	15.86	$0.77 \pm 13/2\rangle + 0.15 \pm 9/2\rangle + 0.05 \pm 11/2\rangle$

*Only the contributions $\geq 5\%$ are given.

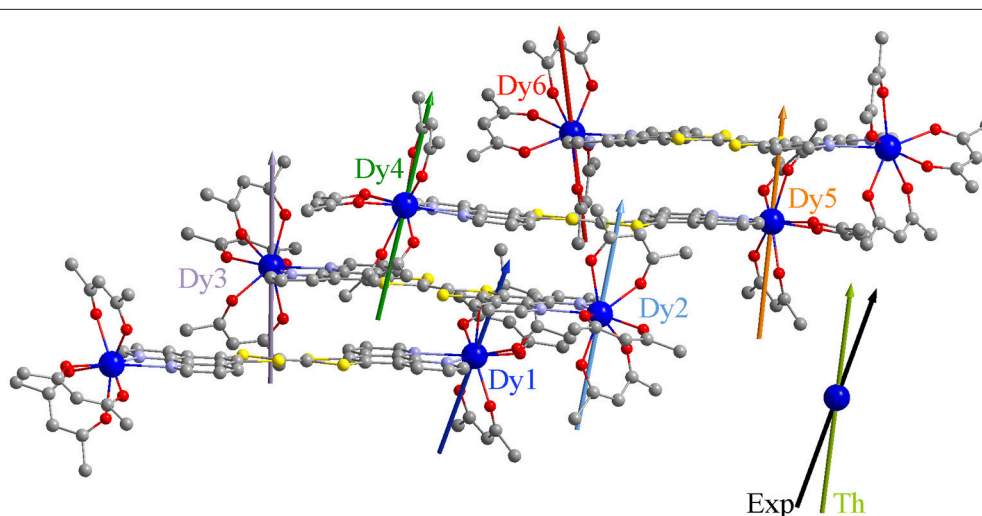
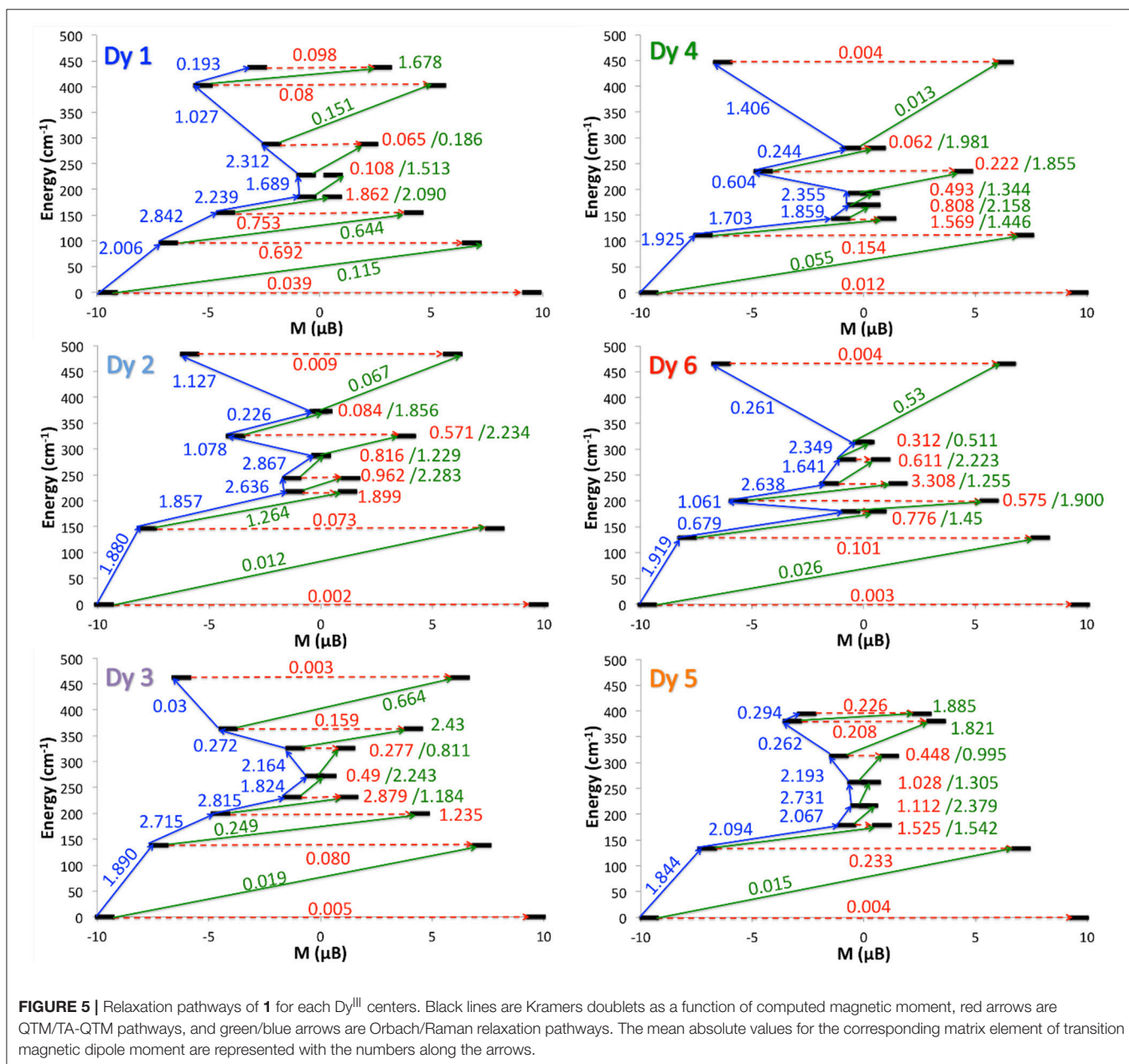


FIGURE 4 | Representation of the crystallographic structure of **1** with the theoretical main anisotropy axes. Colored vectors correspond to the calculated orientations of the largest g-value in the effective spin $\frac{1}{2}$ formalism. The largest g-value determined experimentally is represented with a black arrow and the average calculated orientation in khaki.

are not included in the calculations (Vignesh et al., 2017). Of utmost importance, (i) the coplanar arrangement of the TTF-based ligands is driven by the supramolecular stack through both π - π and donor-acceptor interactions, (ii) previous works on oblate Dy(III) ion in N_2O_6 environment demonstrated the perpendicular orientation of the main anisotropy axis compared to the plan formed by the two nitrogen atoms and thus permit to predict to some extent the parallel direction of all the anisotropy axes.

In order to rationalize the experimental ac magnetic measurements and to identify the three families of Dy centers, the transition matrix elements of the magnetic moment were

computed. The strength of these matrix elements allows to sketch the magnetic relaxation pathway for each Dy ion (Figure 5). It appears that the two Dy1 and Dy4 centers displayed the most efficient QTM and might correspond to the maxima at 5,000 Hz at 2 K. Dy2 and Dy6 are the ions with the most calculated Ising type magnetic anisotropy and the magnetic relaxation may involve the first excited state. They should display the slowest relaxation time with maxima of the out-of-phase component of the magnetic susceptibility centered at 3 Hz. Finally, the intermediate maxima at 315 Hz could be attributed to the Dy3 and Dy5 ions.



CONCLUSIONS

In summary, the redox-active Bis(1,10-phenanthro[5,6-b])tetrathiafulvalene triad (L) was used to bridge two Dy(hfac)₃ units giving the dinuclear complex of formula [Dy₂(hfac)₆(L)]·CH₂Cl₂·C₆H₁₄. The supramolecular organization of the dinuclear species in the crystal driven by the donor-acceptor interactions leads to co-planar stacks of the triads. The coordinated ligands lead to a N₂O₆ environment with a crystal field splitting suitable for the observation of slow magnetic relaxation under an applied magnetic field. In a crystallographic point of view six independent Dy(III) ions have been identified resulting in three families of metal centers displaying different relaxation time of their magnetization in the frequency windows of 1–10 kHz at 2 K. Experimental and the ab-initio study confirmed the Ising nature of the magnetic anisotropy for the Dy(III) ions with the main anisotropy axes perpendicular to the co-planar stacks of the triads. Finally, based on structural analysis, composition of the ground doublet state and probability of QTM, a tentative attribution of the Dy(III) ions to the three different families of field-induced mononuclear SMM was achieved, as out-of-phase signal of the magnetic susceptibility for Dy₂/Dy₆, Dy₃/Dy₅, Dy₁/Dy₄, respectively centered at 3, 315, and 5,000 Hz. The redox-activity of the triad is promising in the perspective to use it as a switch between the mononuclear SMM.

REFERENCES

- Abraham, A., and Bleaney, B. (1970). *Electron Paramagnetic Resonance of Transition Ions*. Oxford: Clarendon Press.
- Adamo, C., and Barone, V. (1999). Toward reliable density functional methods without adjustable parameters: the PBE0 model. *J. Chem. Phys.* 110, 6158–6170. doi: 10.1063/1.478522
- Aquilante, F., Autschbach, J., Carlson, R. K., Chibotaru, L. F., Delcey, M. G., De Vico, L., et al. (2016). MOLCAS 8: new capabilities for multiconfigurational quantum chemical calculations across the periodic table. *J. Comput. Chem.* 37, 506–541. doi: 10.1002/jcc.24221
- Aquilante, F., Malmqvist, P.-A., Pedersen, T.-B., Ghosh, A., and Roos, B. O. (2008). Cholesky decomposition-based multiconfiguration second-order perturbation theory (CD-CASPT2): application to the spin-state energetics of Co^{III}(diiminato)(NPh). *J. Chem. Theory Comput.* 4, 694–702. doi: 10.1021/ct700263h
- Benelli, C., and Gatteschi, D. (2002). Magnetism of lanthanides in molecular materials with transition-metal ions and organic radicals. *Chem. Rev.* 102, 2369–2388. doi: 10.1021/cr010303r
- Bogani, L., and Wernsdorfer, W. (2008). Molecular spintronics using single-molecule magnets. *Nat. Mater.* 7, 179–186. doi: 10.1038/nmat2133
- Chen, B., Lv, Z.-P., Hua, C. F., Leong, C., Tuna, F. M., D'Alessandro, D., et al. (2016). Dinuclear ruthenium complex based on a π-extended bridging ligand with redox-active tetrathiafulvalene and 1,10-phenanthroline units. *Inorg. Chem.* 55, 4606–4615. doi: 10.1021/acs.inorgchem.6b00437
- Chibotaru, L. F., and Ungur, L. (2012). *Ab initio* calculation of anisotropic magnetic properties of complexes. I. unique definition of pseudospin Hamiltonians and their derivation. *J. Chem. Phys.* 137, 064112–064122. doi: 10.1016/1.4739763
- Chibotaru, L. F., Ungur, L., and Soncini, A. (2008). The origin of nonmagnetic kramers doublets in the ground state of dysprosium triangles: evidence for a toroidal magnetic moment. *Angew. Chem. Int. Ed.* 47, 4126–4129. doi: 10.1002/anie.200800283
- Cole, K. S., and Cole, R. H. (1941). Dispersion and absorption in dielectrics I. alternating current characteristics. *J. Chem. Phys.* 9, 341–351. doi: 10.1063/1.1750906
- Comby, S., and Bünzli, J.-C. G. (2007). *Handbook on the Physics and Chemistry of Rare Earths*. Amsterdam: Elsevier BV.
- Cucinotta, G., Perfetti, M., Luzon, J., Etienne, M., Car, P. E., Caneschi, A., et al. (2012). Magnetic anisotropy in a dysprosium/DOTA single-molecule magnet: beyond simple magneto-structural correlations. *Angew. Chem. Int. Ed.* 51, 1606–1610. doi: 10.1002/anie.201107453
- da Cunha, T. T., Jung, J., Boulon, M. E., Campo, G., Pointillart, F., Pereira, C. L. M., et al. (2013). Magnetic poles determinations and robustness of memory effect upon solubilization in a Dy^{III}-based single ion magnet. *J. Am. Chem. Soc.* 135, 16332–16335. doi: 10.1021/ja4089956
- Dolg, M., Stoll, H., and Preuss, H. (1993). A combination of quasirelativistic pseudopotential and ligand field calculations for lanthanoid compounds. *Theor. Chim. Acta* 85, 441–450.
- Dupont, N., Ran, Y.-F., Liu, S.-X., Grilj, J., Vauthey, E., Decurtins, S., et al. (2013). A donor-acceptor tetrathiafulvalene ligand complexed to iron(II): synthesis, electrochemistry, and spectroscopy of [Fe(phen)₃-TTF-dppz](PF₆)₂. *Inorg. Chem.* 52, 306–312. doi: 10.1021/ic3019277
- Ehama, K., Ohmichi, Y., Sakamoto, S., Fujinami, T., Matsumoto, N., Mochida, N., et al. (2013). Synthesis, structure, luminescent, and magnetic properties of carbonate-bridged Z_n^{II}L_n^{III} complexes [(μ₄-CO₃)₂{Zn^{II}L^{III}(NO₃)₂}] (Ln^{III} = Gd^{III}, Tb^{III}, Dy^{III}; L^I = N,N'-Bis(3-methoxy-2-oxybenzylidene)-1,3-propanediaminato, L² = N,N'-Bis(3-ethoxy-2-oxybenzylidene)-1,3-propanediaminato). *Inorg. Chem.* 52, 12828–12841. doi: 10.1021/ic4022273
- Frisch, M. J., Trucks, G. W., Schlegel, H. B., Scuseria, G. E., Robb, M. A., Cheeseman, J. R., et al. (2013). *Gaussian 09, Revision D.01*. Wallingford, CT: Gaussian Inc.
- Ganzhorn, M., Klyatskaya, S., Ruben, M., and Wernsdorfer, W. (2013). Strong spin-phonon coupling between a single-molecule magnet and a carbon nanotube nanoelectromechanical system. *Nat. Nanotechnol.* 8, 165–169. doi: 10.1038/nnano.2012.258

AUTHOR CONTRIBUTIONS

BL and FP made the synthesis; OG and OC performed the magnetic measurements and interpreted them; JF performed single crystal rotating magnetometry; BLG and VM performed the ab initio calculations. All authors participated in the writing process of the manuscript. All authors read and approved the final version of the manuscript.

FUNDING

This work was supported by Région Bretagne, Rennes Métropole, CNRS, Université de Rennes 1, FEDER and the European Research Council (ERC, MULTIPROSM project N° 725184).

ACKNOWLEDGMENTS

BLG and VM thank the French GENCI/IDRIS-CINES center for high-performance computing resources.

SUPPLEMENTARY MATERIAL

The Supplementary Material for this article can be found online at: <https://www.frontiersin.org/articles/10.3389/fchem.2018.00552/full#supplementary-material>

- Gao, F., Cui, L., Liu, W., Hu, L., Zhong, Y. W., Li, Y. Z., et al. (2013). Seven-coordinate lanthanide sandwich-type complexes with a tetrathiafulvalene-fused Schiff base ligand. *Inorg. Chem.* 52, 11164–11172. doi: 10.1021/ic401421h
- Gao, F., Zhang, X. M., Cui, L., Deng, K., Zeng, Q. D., and Zuo, J. L. (2014). Tetrathiafulvalene-supported triple-decker phthalocyaninato dysprosium(III) complex: synthesis, properties and surface assembly. *Sci. Rep.* 4, 5928–5935. doi: 10.1038/srep05928
- Gatteschi, D., and Sessoli, R. (2003) Quantum tunneling of magnetization and related phenomena in molecular materials. *Angew. Chem. Int. Ed.* 42, 268–297. doi: 10.1002/anie.200390099
- Gatteschi, D., Sessoli, R., and Villain, J. (2006). *Molecular Nanomagnets*. New York, NY: Oxford University Press.
- Goodwin, C. A. P., Ortu, F., Reta, D., Chilton, N. F., and Mills, D. P. (2017). Molecular magnetic hysteresis at 60 kelvin in dysprosocenium. *Nature* 548, 439–442. doi: 10.1038/nature23447
- Guo, F. S., Day benjamin, M., Chen, Y. C., Tong, M. L., Mansikkamäki, A., and Layfield, R. A. (2017). A dysprosium metallocene single-molecule magnet functioning at the axial limit. *Angew. Chem. Int. Ed.* 56, 11445–11449. doi: 10.1002/anie.201705426
- Guo, Y. N., Xu, G. F., Gamez, P., Zhao, L., Lin, S. Y., Deng, R., et al. (2010). Two-step relaxation in a linear tetranuclear dysprosium(III) aggregate showing single-molecule magnet behavior. *J. Am. Chem. Soc.* 132, 8538–8539. doi: 10.1021/ja103018m
- Guo, Y. N., Xu, G. F., Wernsdorfer, W., Ungur, L., Guo, Y., Tang, J., et al. (2011). Strong axiality and ising exchange interaction suppress zero-field tunneling of magnetization of an asymmetric Dy₂ single-molecule magnet. *J. Am. Chem. Soc.* 133, 11948–11951. doi: 10.1021/ja205035g
- Gupta, S. K., and Murugavel, R. (2018). Enriching Lanthanide single-ion magnetism through symmetry and axiality. *Chem. Commun.* 54, 3685–3696. doi: 10.1039/C7CC09956H
- Ishikawa, N., Sugita, M., and Wernsdorfer, W. (2005a). Quantum tunneling of magnetization in lanthanide single-molecule magnets: Bis(phthalocyaninato)terbium and Bis(phthalocyaninato)dysprosium Anions. *Angew. Chem. Int. Ed.* 44, 2931–2935. doi: 10.1002/anie.200462638
- Ishikawa, N., Sugita, M., and Wernsdorfer, W. (2005b). Nuclear spin driven quantum tunneling of magnetization in a new lanthanide single-molecule magnet: Bis(Phthalocyaninato)holmium anion. *J. Am. Chem. Soc.* 127, 3650–3651. doi: 10.1021/ja0428661
- Jia, C., Liu, S. X., Tanner, C., Leiggner, C., Neels, A., Sanguinet, L., et al. (2007). An experimental and computational study on intramolecular charge transfer: a tetrathiafulvalene-fused dipyrrophenazine molecule. *Chem. Eur. J.* 13, 3804–3812. doi: 10.1002/chem.200601561
- Jia, H., Ding, J., Hauser, A., Decurtins, S., and Liu, S.-X. (2014). Large π -conjugated chromophores derived from tetrathiafulvalene. *Asian J. Org. Chem.* 3, 198–202. doi: 10.1002/ajoc.201300144
- Kahn, O. (1993). *Molecular Magnetism*. Weinheim: VCH.
- Keniley, L. Jr, Dupont, N., Ray, L., Ding, J., Kovnir, K., Hoyt, M. J., et al. (2013). Complexes with redox-active ligands: synthesis, structure, and electrochemical and photophysical behavior of the Ru(II) complex with TTF-annulated phenanthroline. *Inorg. Chem.* 52, 8040–8052. doi: 10.1021/ic4006949
- Keniley, L. Jr, Ray, L., Kovnir, K. A., and Shatruk, M. (2010). TTF-annulated phenanthroline and unexpected oxidation cleavage of the C=C bond in its ruthenium(II) complex. *Inorg. Chem.* 49, 1307–1309. doi: 10.1021/ic902230f
- Kuropatov, V., Klementieva, S., Fukin, G., Mitin, A., Ketlov, S., Budnikova, Y., et al. (2010). Novel method for the synthesis of functionalized tetrathiafulvalenes, an acceptor-donor-acceptor molecule comprising of two o-quinone moieties linked by a TTF bridge. *Tetrahedron* 66, 7605–7611. doi: 10.1016/j.tet.2010.07.038
- Lapadula, G., Trummer, D., Conley, M. P., Steinmann, M., Ran, Y.-F., Brasselet, S., et al. (2015). One-photon near-infrared sensitization of well-defined Yb(III) surface complexes for NIR-to-NIR single nanoparticle imaging. *Chem. Mater.* 27, 2033–2039. doi: 10.1021/acs.chemmater.5b00306
- Lehmann, J., Gaita-Arino, A., Coronado, E., and Loss, D. (2007). Spin qubits with electrically gated polyoxometalate molecules. *Nat. Nanotechnol.* 2, 312–317. doi: 10.1038/nnano.2007.110
- Leuenberger, M. N., and Loss, D. (2001). Quantum computing in molecular magnets. *Nature* 410, 789–793. doi: 10.1038/35071024
- Liddle, S. T., and van Slageren, J. (2015). Improving f-element single molecule magnets. *Chem. Soc. Rev.* 44, 6655–6669. doi: 10.1039/C5CS00222B
- Llunell, M., Casanova, D., Cirera, J., Bofill, J. M., Alemany, P., and Alvarez, S. (2013). *SHAPE (v. 2.1)*. Barcelona.
- Long, J., Rouquette, J., Thibaud, J. M., Ferreira, R. A. S., Carlos, L. D., Donnadieu, B., et al. (2015). A high-temperature molecular ferroelectric Zn/Dy complex exhibiting single-ion-magnet behavior and lanthanide luminescence. *Angew. Chem. Int. Ed.* 54, 2236–2240. doi: 10.1002/anie.201410523
- Long, J., Vallat, R., Ferreira, R. A., Carlos, L. D., Paz, F. A. A., Guari, Y., et al. (2012). A bifunctional luminescent single-ion magnet: towards correlation between luminescence studies and magnetic slow relaxation processes. *Chem. Commun.* 48, 9974–9976. doi: 10.1039/C2CC35321K
- Lu, J., Guo, M., and Tang, J. (2017). Recent developments in lanthanide single-molecule magnets. *Chem. Asian J.* 12, 2772–2779. doi: 10.1002/asia.201701032
- Malmqvist, P. A., and Roos, B. O. (1989). The CASSCF state interaction method. *Chem. Phys. Lett.* 155, 189–194. doi: 10.1016/0009-2614(89)85347-3
- Malmqvist, P. A., Roos, B. O., and Schimmelpennig, B. (2002). The restricted active space (RAS) state interaction approach with spin-orbit coupling. *Chem. Phys. Lett.* 357, 230–240. doi: 10.1016/S0009-2614(02)00498-0
- Mannini, M., Pineider, F., Sainctavit, P., Danieli, C., Otero, E., Sciancalepore, C., et al. (2009). Magnetic memory of a single-molecule quantum magnet wired to a gold surface. *Nat. Mater.* 8, 194–197. doi: 10.1038/nmat2374
- Nishida, J. I., Kumaki, D., Tokito, S., and Yamashita, Y. (2006). High performance n- and p-type field-effect transistors based on tetrathiafulvalene derivatives. *J. Am. Chem. Soc.* 128, 9598–9599. doi: 10.1021/ja0630083
- Orbach, R. (1961a). Spin-lattice relaxation in rare-earth salts. *Proc. R. Soc. Lond. A Math. Phys. Eng. Sci.* 264, 458–484. doi: 10.1098/rspa.1961.0211
- Orbach, R. (1961b). On the theory of spin-lattice relaxation in paramagnetic salts. *Proc. Phys. Soc.* 77, 821–826.
- Otón, F., Lloveras, V., Mas-Torrent, M., Vidal-Gancedo, J., Veciana, J., and Rovira, C. (2011a). Coupling tetracyanoquinodimethane to tetrathiafulvalene: a fused TCNQ-TTF-TCNQ triad. *Angew. Chem. Int. Ed.* 50, 10902–10906. doi: 10.1002/anie.201104841
- Otón, F., Pfattner, R., Pavlica, E., Olivier, Y., Bratina, G., and , Cornil, J., et al. (2011b). Electronic and structural characterization of a tetrathiafulvalene compound as a potential candidate for ambipolar transport properties. *CrystEngComm* 13, 6597–6600. doi: 10.1039/C1CE05559C
- Ou-Yang, J. K., Saleh, N., Fernandez Garcia, G., Norel, L., Pointillart, F., Guizouarn, T., et al. (2016). Improved slow magnetic relaxation in optically pure helicene-based Dy^{III} single molecule magnets. *Chem. Commun.* 52, 14474–14477. doi: 10.1039/C6CC08638A
- Perdew, J. P., Burke, K., and Ernzerhof, M. (1996). Generalized gradient approximation made simple. *Phys. Rev. Lett.* 77, 3865–3868. doi: 10.1103/physrevlett.77.3865
- Piguet, C., and Bünzli, J.-C. G. (1999). Mono- and polynuclear lanthanide-containing functional assemblies: a field between tradition and novelty. *Chem. Soc. Rev.* 28, 347–358. doi: 10.1039/A804240C
- Pointillart, F., Bernot, K., Golhen, S., Le Guennic, B., Guizouarn, T., Ouahab, L., et al. (2015a). Magnetic memory in an isotopically enriched and magnetically isolated mononuclear dysprosium complex. *Angew. Chem. Int. Ed.* 54, 1504–1507. doi: 10.1002/anie.201409887
- Pointillart, F., Cador, O., Le Guennic, B., and Ouahab, L. (2017). Uncommon Lanthanide ions in purely 4f single molecule magnets. *Coord. Chem. Rev.* 346, 150–175. doi: 10.1016/j.ccr.2016.12.017
- Pointillart, F., Golhen, S., Cador, O., and Ouahab, L. (2013a). Paramagnetic 3d coordination complexes involving redox-active tetrathiafulvalene derivatives: an efficient approach to elaborate multi-properties materials. *Dalton Trans.* 42, 1949–1960. doi: 10.1039/c2dt32150e
- Pointillart, F., Jung, J., Berraud-Pache, R., Le Guennic, B., Dorcet, V., Golhen, S., et al. (2015b). L. luminescence and single-molecule magnet behavior in lanthanide complexes involving a tetrathiafulvalene-fused dipyrrophenazine ligand. *Inorg. Chem.* 54, 5384–5397. doi: 10.1021/acs.inorgchem.5b00441

- Pointillart, F., Le Guennic, B., Cador, O., Maury, O., and Ouahab, L. (2015c). Lanthanide ion and tetrathiafulvalene-based ligand as a “magic” Couple toward luminescence, single molecule magnets, and magnetostructural correlations. *Acc. Chem. Res.* 48, 2834–2842. doi: 10.1021/acs.accounts.5b00296
- Pointillart, F., Le Guennic, B., Golhen, S., Cador, O., Maury, O., and Ouahab, L. (2013b). A redox-active luminescent ytterbium based single molecule magnet. *Chem. Commun.* 49, 615–617. doi: 10.1039/C2CC37635K
- Pointillart, F., Liu, X., Kepenekian, M., Le Guennic, B., Golhen, S., Dorcet, V., et al. (2016). Thermal and near-infrared light induced spin crossover in a mononuclear iron(II) complex with a tetrathiafulvalene-fused dipyrrophenazine ligand. *Dalton Trans.* 45, 11267–11271. doi: 10.1039/C6DT00920D
- Qin, J., Hu, L., Li, G. N., Wang, X. S., Xu, Y., et al. (2011). Synthesis, characterization, and properties of rhenium(I) tricarbonyl complexes with tetrathiafulvalene-fused phenanthroline ligands. *Organometallics* 30, 2173–2179. doi: 10.1021/om101141h
- Ren, M., Bao, S. S., Ferreira, R. A., Zheng, L. M., and Carlos, L. D. (2014). A layered erbium phosphonate in pseudo-D_{5h} symmetry exhibiting field-tunable magnetic relaxation and optical correlation. *Chem. Commun.* 50, 7621–7624. doi: 10.1039/C4CC02085E
- Richardson, M. F., Wagner, W. F., and Sands, D. E. (1968). Rare-earth tris(hexafluoroacetylacetonates) and related compounds. *J. Inorg. Nucl. Chem.* 30, 1275–1289. doi: 10.1016/0022-1902(68)80557-3
- Rinehart, J. D., and Long, J. R. (2011). Exploiting single-ion anisotropy in the design of f-element single-molecule magnets. *Chem. Sci.* 2, 2078–2085. doi: 10.1039/C1SC00513H
- Roos, B. O., Lindh, R., Malmqvist, P.-A., Veryazov, V., and Widmark, P.-O. (2004). Main group atoms and dimers studied with a new relativistic ANO basis set. *J. Phys. Chem. A* 108, 2851–2858. doi: 10.1021/jp031064+
- Roos, B. O., Lindh, R., Malmqvist, P.-A., Veryazov, V., and Widmark, P.-O. (2005). New relativistic ANO basis sets for transition metal atoms. *J. Phys. Chem. A* 109, 6575–6579. doi: 10.1021/jp0581126
- Roos, B. O., Lindh, R., Malmqvist, P. A., Veryazov, V., Widmark, P. O., and Borin, A. C. (2008). New relativistic atomic natural orbital basis sets for lanthanide atoms with applications to the Ce diatom and LuF₃. *J. Phys. Chem. A* 112, 11431–11435. doi: 10.1021/jp803213j
- Roos, B. O., Taylor, P. R., and Siegbahn, P. E. M. (1980). A complete active space SCF method (CASSCF). using a density matrix formulated super-CI approach. *Chem. Phys.* 48, 157–288. doi: 10.1016/0301-0104(80)80045-0
- Schuler, B., Liu, S. X., Geng, Y., Decurtins, S., Meyer, G., and Gross, L. (2014). Contrast formation in kelvin probe force microscopy of single π -conjugated molecules. *Nano Lett.* 14, 3342–3346. doi: 10.1021/nl500805x
- Scott, P. L., and Jeffries, C. D. (1962). Spin-lattice relaxation in some rare-earth salts at helium temperatures; observation of the phonon bottleneck. *Phys. Rev.* 127, 32–51. doi: 10.1103/PhysRev.127.32
- Sessoli, R., and Powell, A. K. (2009). Strategies towards single molecule magnets based on lanthanide ions. *Coord. Chem. Rev.* 253, 2328–2341. doi: 10.1016/j.ccr.2008.12.014
- Sheldrick, G. M. (2015a). SHELXT – Integrated space-group and crystal-structure determination. *Acta Crystallogr. Sect. A Found Adv.* 71, 3–8. doi: 10.1107/S2053273314026370
- Sheldrick, G. M. (2015b). Crystal structure refinement with SHELXL. *Acta Crystallogr. Sect. C* 71, 3–8. doi: 10.1107/S2053229614024218
- Shrivastava, K. N. (1983). Theory of spin–lattice relaxation. *Phys. Status Solidi* 117, 437–458. doi: 10.1002/pssb.2221170202
- Soussi, K., Jung, J., Pointillart, F., Le Guennic, B., Lefevre, B., Golhen, S., et al. (2015). Magnetic and photo-physical investigations into DyIII and YbIII complexes involving tetrathiafulvalene ligand. *Inorg. Chem. Front.* 2, 1105–1117. doi: 10.1039/C5QI00087D
- Speed, S., Feng, M., Fernandez Garcia, G., Pointillart, F., Lefevre, B., Riobé, F., et al. (2017). Lanthanide complexes involving multichelating TTF-based ligands. *Inorg. Chem. Front.* 4, 604–617. doi: 10.1039/c6qi00546b
- Vignesh, K. R., Langley, S. K., Murray, K. S., and Rajaraman, G. (2017). Exploring the influence of diamagnetic ions on the mechanism of magnetization relaxation in {Co^{III}Ln^{III}} (Ln = Dy, Tb, Ho). “butterfly” complexes. *Inorg. Chem.* 56, 2518–2532. doi: 10.1021/acs.inorgchem.6b02720
- Weigend, F., and Ahlrichs, R. (2005). Balanced basis sets of split valence, triple zeta valence and quadruple zeta valence quality for H to Rn: design and assessment of accuracy. *Phys. Chem. Chem. Phys.* 7, 3297–3305. doi: 10.1039/b508541a
- Woodruff, D. N., Winpenny, R. E. P., and Layfield, R. A. (2013). Lanthanide single-molecule magnets. *Chem. Rev.* 113, 5110–5148. doi: 10.1021/cr400018d
- Yamashita, K., Miyazaki, R., Kataoka, Y., Nakanishi, T., Hasegawa, Y., Nakano, M., et al. (2013). A luminescent single-molecule magnet: observation of magnetic anisotropy using emission as a probe. *Dalton Trans.* 42, 1987–1990. doi: 10.1039/C2DT32785F
- Yi, X., Bernot, K., Le Corre, V., Calvez, G., Pointillart, F., Cador, O., Le Guennic, B., et al. (2014). Unraveling the crystal structure of lanthanide-murexide complexes: use of an ancient complexometry indicator as a near-infrared-emitting single-ion magnet. *Chem. Eur. J.* 20, 1569–1576. doi: 10.1002/chem.201303833
- Zhang, L., Jung, J., Zhang, P., Guo, M., Zhao, L., Tang, J., et al. (2016). Site-resolved two-step relaxation process in an asymmetric Dy₂ single-molecule magnet. *Chem. Eur. J.* 22, 1392–1398. doi: 10.1002/chem.201503422
- Zhang, P., Zhang, L., and Tang, J. (2015). Lanthanide single molecule magnets: progress and perspective. *Dalton Trans.* 44, 3923–3929. doi: 10.1039/C4DT03329A
- Zhu, Z., Guo, M., Li, X.-L., and Tang, J. (2019). Molecular magnetism of lanthanide: advances and perspectives. *Coord. Chem. Rev.* 378, 350–364. doi: 10.1016/j.ccr.2017.10.030

Conflict of Interest Statement: The authors declare that the research was conducted in the absence of any commercial or financial relationships that could be construed as a potential conflict of interest.

Copyright © 2018 Lefevre, Galangau, Gonzalez, Montigaud, Dorcet, Ouahab, Le Guennic, Cador and Pointillart. This is an open-access article distributed under the terms of the Creative Commons Attribution License (CC BY). The use, distribution or reproduction in other forums is permitted, provided the original author(s) and the copyright owner(s) are credited and that the original publication in this journal is cited, in accordance with accepted academic practice. No use, distribution or reproduction is permitted which does not comply with these terms.